Acta Materialia 155 (2018) 410–417

Contents lists available at ScienceDirect

Acta Materialia

journal homepage: www.elsevier.com/locate/actamat

Full length article

Radiation damage reduction by grain-boundary biased defect migration in nanocrystalline Cu

Miaomiao Jin [a], Penghui Cao [a, *], Sidney Yip [a, b], Michael P. Short [a]

[a] Department of Nuclear Science and Engineering, Massachusetts Institute of Technology, Cambridge, MA, 02139, USA
[b] Department of Materials Science and Engineering, Massachusetts Institute of Technology, Cambridge, MA, 02139, USA

ARTICLE INFO

Article history:
Received 1 March 2018
Received in revised form
1 May 2018
Accepted 29 May 2018
Available online 14 June 2018

Keywords:
Nanocrystalline metal
Grain boundary
Damage reduction mechanisms
Self-healing
Stacking fault tetrahedron

ABSTRACT

Nanocrystalline materials with a high density of grain boundaries have long been reported to alleviate radiation damage. However, a full mechanistic understanding of defect reduction, particularly the interaction mechanisms between grain boundaries and clustered defects during irradiation, remains an open question. Here we present atomistic simulations of prolonged radiation damage evolution in Cu bicrystals with increasing radiation dose. Our results reveal the atomic details of defect nucleation and migration, and the mechanisms for the annihilation of defect clusters during irradiation. Stacking fault tetrahedra formed due to radiation damage cascades show preferential migration to irradiated grain boundary. Interstitial-loaded grain boundaries are observed to be dynamically resilient, and persistently interact with the stacking fault tetrahedra, revealing a self-healing response to radiation damage. The results show a synergistic effect of grain boundaries on defect annihilation at small grain spacings of less than 6 nm, giving rise to a drastic decrease in the density of defect clusters. These findings, along with the mechanistic insights, present an integrated perspective on interface-mediated damage reduction in radiation-resistant nanomaterials.

1. Introduction

Nanostructured materials in the form of nanocrystalline [1], nanolayered [2], nanoporous [3], and nanodispersed [4] structures have received much attention due to their exceptional tolerance of radiation damage compared with their coarse-grained counterparts [5]. During irradiation, point defects including vacancies, interstitials, and defect clusters are produced by displacement cascades [6]. These defects further migrate and aggregate, forming larger clusters such as dislocation loops, interstitial clusters, stacking fault tetrahedra (SFTs) [7,8], and voids [9]. The continual alteration of the microstructure due to radiation damage leads to severe degradation of material properties, including radiation hardening [10,11], embrittlement [12], creep and swelling [13], and eventual material failure. In nanocrystalline (NC) materials, the high fraction of grain boundaries (GBs) or interfaces serve as defect sinks, ultimately contributing to defect reduction. Recently, NC materials have been intensely studied by *in situ* [14–17] and *ex situ* [1,18] ion irradiation experiments. It has been found that NC materials exhibit smaller defect sizes and lower defect densities than their polycrystalline counterparts [17,19]. Moreover, the defect cluster density shows strong dependence on the average GB spacing, with a more refined nanostructure giving rise to a lower defect density. It is reasonable to attribute these changes to GB-mediated defect annihilation, such as SFTs absorbed during their interaction with twin boundaries [16,20]. Despite these successful experiments, the mechanistic understanding of GB-mediated SFT annihilation in these materials was not fully elucidated, mostly due to the inability to resolve the complexity at the atomic level.

To unravel the mechanisms of GB-mediated point defect annihilation, a number of atomistic simulations have explored how collision cascades interact with GBs. The influence of GBs on defect production was extensively investigated by many groups, including Samaras et al. [21,22], Bai and Uberuaga et al. [23,24], and Demkowicz et al. [25]. The GBs act as defect containers by preferentially absorbing collision cascade-produced interstitials. As a result, defect distributions are strongly biased by the GBs, leaving behind vacancy-rich bulk regions and interstitial-concentrated GBs [5,22,26]. The interstitial-rich GBs lower the energetic barriers to interstitial migration and efficiently emit interstitials to interact with nearby vacancies, leading to enhanced interstitial-vacancy

* Corresponding author.
E-mail address: pcao@mit.edu (P. Cao).

https://doi.org/10.1016/j.actamat.2018.05.071
1359-6454/

recombination processes [23,27].

In addition to point defects, clustered defects such as SFTs are predominant in many irradiated face centered cubic (FCC) metals, including Cu, Ag, Ni, and Au [20,28]. Dislocation pinning by these radiation-induced defect clusters increases the resistance to plastic flow, causing material hardening and embrittlement [11]. Therefore, their reduction or removal is key to radiation damage resistance. For these reasons, the interaction of SFTs with various types of pristine GBs has been simulated [29–31], and the ability to remove SFTs depends on the GB's structural characteristics. Despite the successes of previous atomistic simulations, the detailed mechanisms of SFT interaction with GBs as a function of irradiation dose and their mechanisms for damage reduction in NC materials remain elusive, because the microscopic structures of the GBs themselves constantly change under irradiation.

Essentially, the way in which defects interact with irradiated GBs is different from that with pristine GBs and interfaces [5,24]. For a comprehensive understanding of damage reduction and the enhanced radiation-tolerance in NC materials, we develop a consecutive displacement cascade algorithm to perform atomistic simulations of prolonged radiation damage in NC-Cu, a system that has been widely used in irradiation studies [14,17,23,25,32]. The aims of this work are to understand (1) radiation-induced defect evolution with increasing damage dose, particularly defect cluster nucleation, migration and aggregation in the presence of GBs, (2) the mechanisms and processes for SFT annihilation, and (3) how radiation-induced defect density depends on grain size.

2. Computational models and methods

We consider two representative, high-angle $\Sigma5(210)$ and $\Sigma5(310)$ symmetrical tilt GBs in Cu, modeled by an embedded-atom method (EAM) potential developed by Mishin et al. [33]. In Fig. 1 (a), we show the simulation model used in this study, with periodic boundary conditions applied in all three directions. The GBs in the simulation cell are separated by a spacing λ. The lengths of the simulation box along $X-$, $Y-$, and $Z-$ directions are $2\lambda \times 11.4\,\text{nm} \times 10.9\,\text{nm}$, with λ ranging from 5.7 nm to 28.5 nm considered, corresponding to between 117,600 and 588,000 atoms. The GB is built by joining two perfect crystals along the (210) or (310) planes followed by static energy minimization. A number of configurations are sampled by varying the relative positions of the two crystals and removing atoms within a cutoff distance, which is varied to obtain an equilibrium state. The stable structures with the lowest potential energy in each configuration are chosen for this study. Fig. 1(b) and (c) show the equilibrium structures of the two symmetrical boundaries $\Sigma5(210)$ and $\Sigma5(310)$, respectively. In the figure, we highlight the structural units [34] to illustrate the boundary characteristics, where both GBs appear to be composed of kite-shaped units [27,35,36]. Atoms are color-coded according to their volumes calculated by Voronoi analysis [37]. It is worth noting that atoms in the GBs indicate larger free volumes than those in the bulk, implying potential sites for accommodating interstitials.

To reach a high damage dose and reveal defect evolution during irradiation, we utilize a recently developed successive displacement cascade algorithm [38] and the molecular dynamics (MD) method as implemented in LAMMPS [39]. The Ziegler-Biersack-Littmark (ZBL) repulsive potential [32,40] is smoothly joined to the aforementioned EAM potential [23] to deal with high energy atom collisions, and an adaptive time step algorithm is used to limit atomic movement to 0.05 Å per timestep. Before the collision cascade simulation, we first relax the system to zero pressure at 300 K for 100 ps. Then, an atom is randomly chosen as the PKA, and the entire system is shifted so that the PKA is positioned at the center of the cell. This operation prevents the damage cascade from reaching the cell boundaries. The PKA is assigned a kinetic energy of 5 keV with a random incident direction, and 50,000 adaptive timesteps (~45 ps) are performed. The Nosé-Hoover temperature-rescaling thermostat [41,42] is applied to the atoms at all sides of the simulation cell with a width of one lattice constant, mimicking a thermal sink to absorb excess collision cascade energy and cool the system to 300 K. To clearly uncover defect evolution, the system is shifted back after annealing each cascade, allowing defects to be continuously tracked with increasing damage dose. This simulation procedure is repeated with each PKA randomly chosen and shifted to the center of the cell, simulating the spatially random damage cascades. A damage level of ~ 0.27 dpa (250–1250 cascades depending on system size) is achieved according to the NRT approximation i.e. $n \times E_{\text{PKA}}/2E_{\text{D}}$, where n is number of cascades, E_{PKA} is the PKA energy, and E_{D} represents the displacement threshold energy [43]. The short simulation time (an inherent limitation of MD) between collision cascades yields a dose rate several orders of magnitude higher than that in experiments. Although the difference in dose rate between MD and experiments is quite large, recent studies using similar simulation approaches have shown good agreement with experiments [38]. It should be noted that the chosen incident energy of 5 keV is a representative value from the full PKA spectrum in irradiation experiments at MeV energies [44]. This energy enables a reasonably sized simulation cell to reach a damage level comparable to experiments, and allows us to efficiently study defect evolution and diffusion processes and the underlying SFT annealing mechanisms with the presence of GBs.

To illustrate defect nucleation and evolution after each displacement cascade, we use the recently developed method of *in situ* computational microscopy [45,46]. Adaptive common neighbor analysis (*a*-CNA) [47] and the Wigner-Seitz cell method [32] are utilized to identify defective structures and defect types. Specifically, the evolution of interstitials and vacancies is analyzed by comparing irradiated structured with the initially perfect one. All data files supporting the findings of this study, including data files, processing scripts, and accumulated data to produce the figures are available on our public GitHub data repository [48].

3. Results

3.1. Dynamic evolution of defects during irradiation

The results of radiation damage in NC-Cu with $\Sigma5(210)$ GBs are presented in Fig. 2, where defective structures (non-FCC atoms) are shown at various doses. Similar results and defect evolution for $\Sigma5(310)$ GBs is shown in the Supporting Information (*SI*). At a low damage level of 0.001 dpa, one can see in Fig. 2(a) the production of points defects and small clusters, which cause the left-hand GB to wiggle due to its preferential absorption of interstitials. This preferential uptake of interstitials by GBs results in a biased defect distribution, with a vacancy-rich bulk and interstitial-loaded boundary region (distributions of vacancies and interstitials are shown in Fig. S1 of *SI*). As the damage level increases, small defects are continuously produced and the interstitials continue to gather in the boundary region. The GBs in Fig. 2(b) can be regarded as highly irradiated, which appear thicker when compared with pristine ones. They are observed to be more dynamically interactive with surrounding defect clusters, such as SFTs formed through collision cascades or vacancy aggregation. These SFTs preferentially diffuse towards GBs and interact with them as shown in Fig. 2(c),

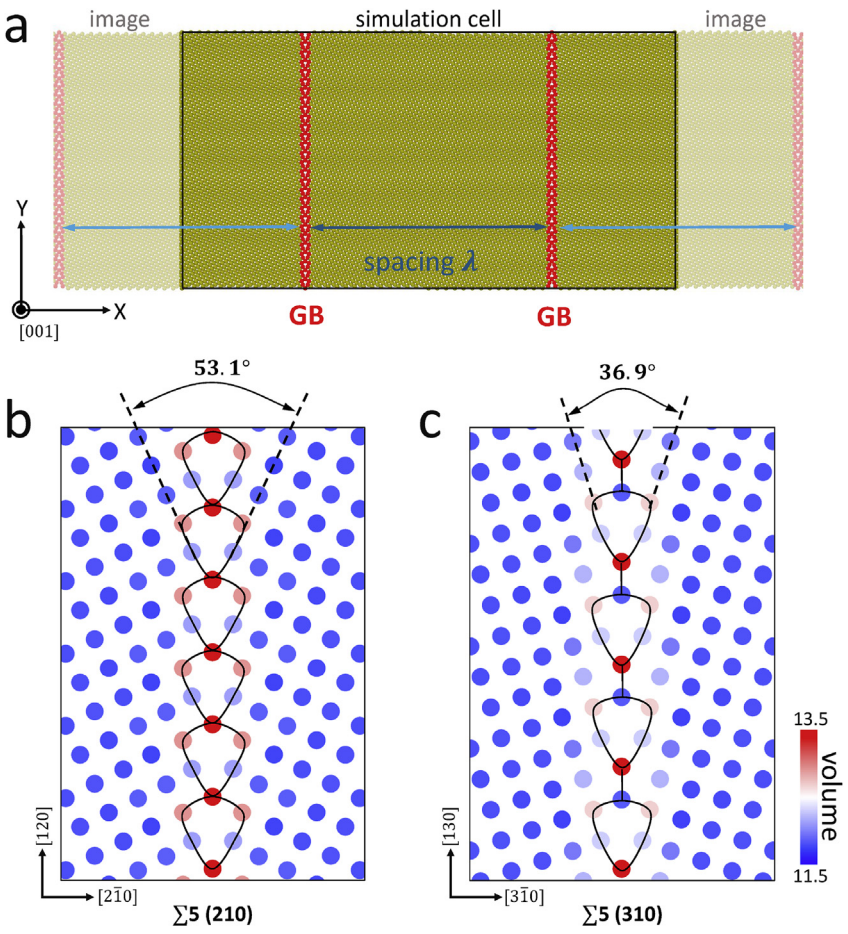

Fig. 1. (a) Illustration of the simulation model used in this study. Brown atoms have a FCC structure, while GB atoms are shown in red. Periodic boundary conditions are applied in all three directions, with periodicity along the x-direction plotted to show GBs separated by a spacing λ. (b–c) GB structures and atomic volume. The GBs structures of $\Sigma5(210)$ (b) and $\Sigma5(310)$ (c) are viewed along the [001] axis. The kite-shaped units are marked to illustrate the GB structures, where atoms are colored by the volume of their Voronoi cells. The misorientation angle is defined by the [100] direction of the two crystals. (For interpretation of the references to color in this figure legend, the reader is referred to the Web version of this article.)

eventually being removed in Fig. 2(d) (the detailed SFT removal process is shown in Fig. S2 of *SI*). At the higher damage level of 0.221 dpa, we do not see a clear increase in SFTs compared with 0.079 dpa, implying that the defect density may have saturated (see discussion of Fig. 3). During irradiation, we also observed that GBs oscillate, sweeping up nearby defects, further contributing to damage reduction. The full details of damage processes and the role of GBs in defect annihilation are illustrated in the supplementary videos.

Supplementary videos related to this article can be found at https://doi.org/10.1016/j.actamat.2018.05.071.

The total number of defective atoms (non-FCC) induced by irradiation as a function of dose is shown in Fig. 3(a). The defect number rapidly increases with doses up to about 0.08 dpa, after which the defect production rate markedly slows, approaching saturation. Both GB types show essentially the same defect accumulation behavior, while $\Sigma5(210)$ has a slightly lower saturated defect density than that of $\Sigma5(310)$, which could be attributed to the extra free volume (Fig. 1(b)) and higher energy of $\Sigma5(210)$ [49]. A similar two-stage process has been observed for the behavior of SFTs in Fig. 3(b). However, SFT saturation appears to reach a slightly higher dose compared with that for the total number of defective atoms, because the system requires extra time to rearrange vacancies into SFTs. After about 0.1 dpa, the number of SFTs starts to fluctuate with a characteristic zigzag shape, suggesting a dynamic equilibrium between SFT creation and annihilation.

3.2. Mechanisms of SFT annihilation

We now focus on the atomistic mechanisms underlying the removal of SFTs, as they constitute one key to understanding the enhanced damage-tolerance of NC metals. It should be noted the following results are described for $\Sigma5(210)$ GBs, whereas the same behavior is also present in $\Sigma5(310)$ ones. The formation of SFTs during irradiation is mainly caused by defect aggregation and vacancy-void self-reorganization [50]. The predominant SFT defects are commonly known to be immobile and stable, with their energetic stability increasing with their size [51,52]. In a recent study, it was found contrary to common belief that even large, defective SFTs are quite mobile, and their diffusivities can be even higher than that of mono-vacancies [53]. Thus the population of various types of SFTs produced under irradiation can be important to understand the radiation resistance and performance of NC-Cu. We analyze the statistical size distributions of SFTs formed during irradiation, where the size of each is measured using the Wigner-Seitz cell method by the number of constituent vacancies [32]. The results are shown in Fig. 4(a). All the defects have been grouped into three categories: perfect SFTs, defective SFTs, and mono- and di-vacancies, where the sizes of perfect SFTs are so-called magic numbers [50]. We find more than 82% of the SFTs are defective in

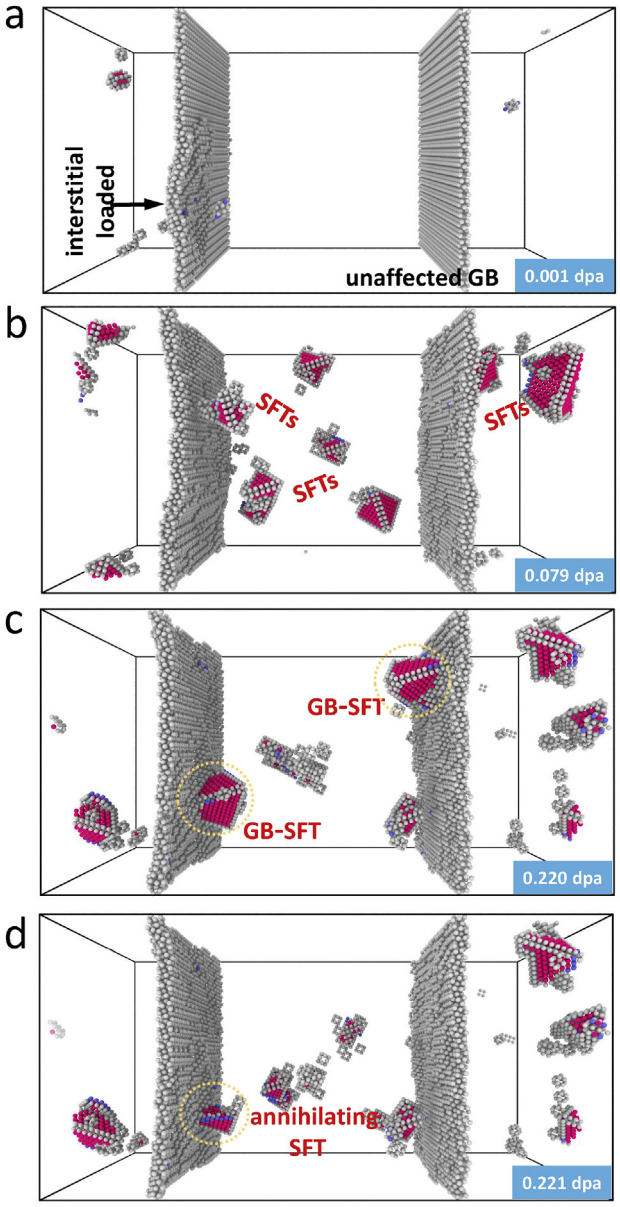

Fig. 2. Radiation-induced defect clusters and GB evolution in Σ5(210) Cu at different doses. The grain spacing λ is 11.4 nm. Atoms are color coded according to their structures (red → HCP, blue → BCC, grey → other structure, FCC atoms not shown). For the sake of clarity, only the ten largest defects are shown in the figures. (a) Point defects and interstitial-loaded GB produced at a low radiation dose of 0.001 dpa (two collision cascades at 5 keV). (b) Irradiated GBs and radiation-induced SFTs at 0.079 dpa. (c–d) indicate that SFTs do not appear to grow in size and number at higher doses, as they are observed interact with GBs where they annihilate. Abbreviations: FCC, face centered cubic; HCP, hexagonal close packed; BCC, body centered cubic; GB, grain boundary; SFTs, stacking fault tetrahedra. (For interpretation of the references to color in this figure legend, the reader is referred to the Web version of this article.)

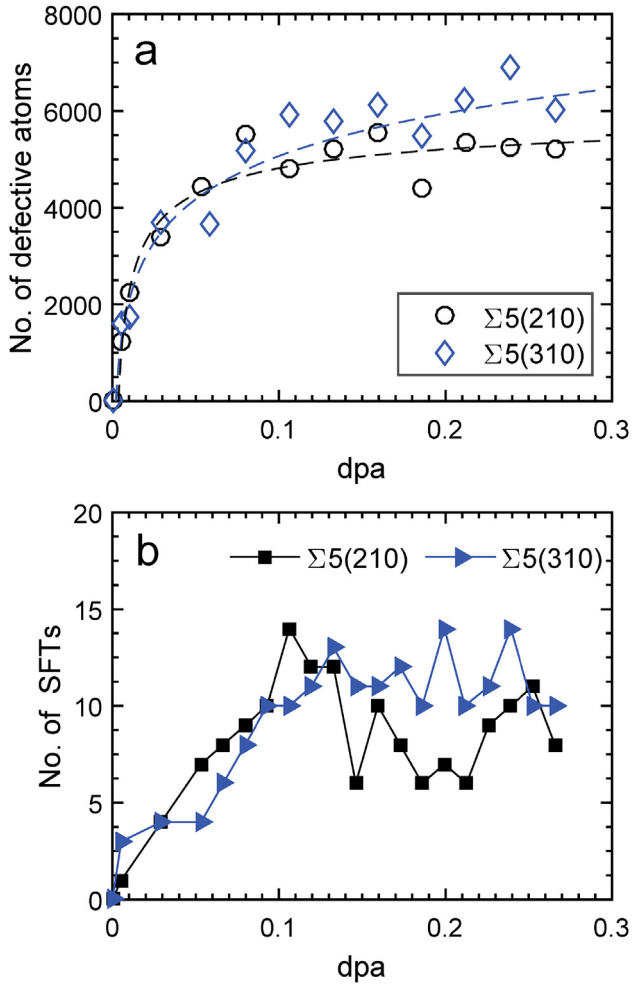

Fig. 3. (a) Total number of defective (non-FCC) atoms as a function of dose in Σ5(210) and Σ5(310) systems. The dashed-lines are shown to guide the reader. (b) Number of large SFTs (clusters containing more than 15 vacancies) versus dose.

the irradiated systems, and their diffusivities, depending on their size, are several orders of magnitude higher than those of the perfect SFTs [53]. The strong heterogeneity of SFT diffusion is evident as shown in the supplementary videos.

By probing the atomistic processes of defect evolution, two typical SFT annihilation modes, removal by GBs and elimination through interstitial recombination, are derived, and their occurrence depends on the corresponding SFT mobility. In consideration of the fact that most SFTs are defective and mobile, GB removal is found to be the major mechanism for SFT annihilation in NC-Cu.

Fig. 4(b) illustrates such a process of removing an SFT via interaction with a GB. A mobile SFT is formed 4.5 nm away from the boundary, which at first appears to be straight. After a short time, the SFT quickly migrates towards this interstitial-loaded GB, while the GB atoms rearrange themselves to accommodate the incoming SFT. In the middle panel of Fig. 4(b), one can see that the distorted GB and the SFT are in direct contact, suggesting an attractive interaction between the irradiated-GB and the SFT. In the meantime, a tensile strain field develops well below the distorted GB. Following SFT annihilation, the GB once again becomes straight in appearance, revealing a resilient, self-healing response to radiation damage [16]. It is expected that the interstitial-loaded GBs will reduce the defect diffusion barrier, allowing interstitials to migrate readily to redistribute themselves along the GB region to facilitate the GB-SFT interaction. The SFT migration during irradiation is not purely random, but shows some bias towards the GBs. This biased SFT diffusion implies attractive forces between interstitial-load GBs and SFTs. Such preferential drift of radiation defects towards GBs and subsequent self-healing interactions lead to radiation damage reduction, with a similar mechanism observed in the interaction between point defects and interfaces [54].

The second annihilation mechanism of interstitial recombination occurs mostly in less mobile clusters, such as perfect SFTs whose diffusivities can be several orders of magnitude lower than

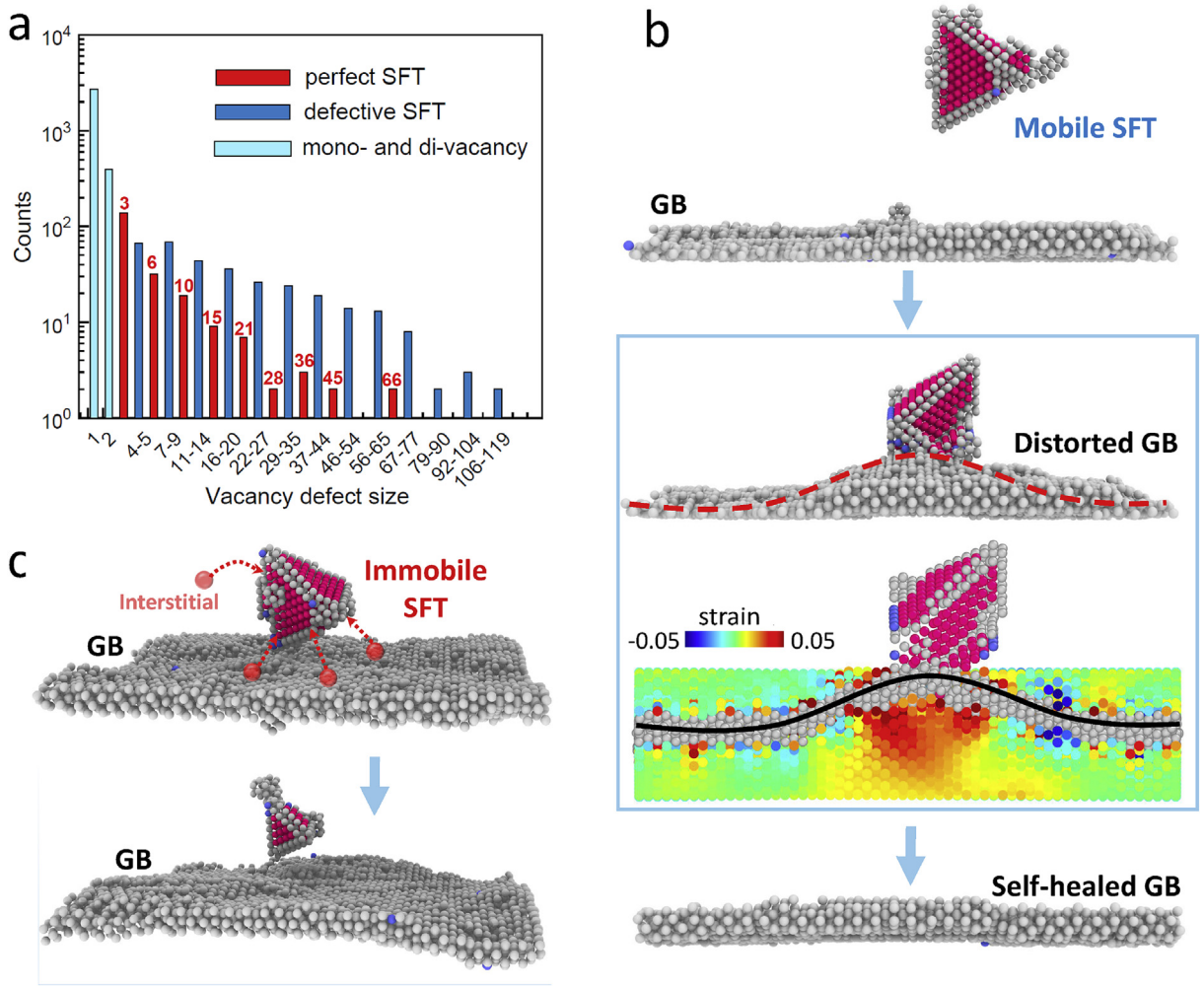

Fig. 4. (a) Statistical distribution of vacancy-type defect sizes in irradiated Σ5(210) Cu with grain spacing of 11.4 nm at damage dose from 0.06 dpa to 0.27 dpa. Mono- and di-vacancies, defective SFTs, and perfect SFTs are grouped and shown according to their sizes (number of vacancies). (b) SFT annihilation process via interaction with a GB. A radiation-induced SFT (upper panel) migrates to a GB, which becomes locally distorted upon contact (middle panel). A cross-sectional view is also provided where neighboring atoms of the GB are colored by atomic strain. Finally, the SFT is absorbed, returning the distorted GB to a straight profile (bottom panel). (c) SFT annihilation by interstitial recombination. An immobile SFT shrinks in size due to absorbing interstitials resulting from GB emission and nearby cascades.

those of defective ones. Fig. 4(c) illustrates the annihilation process, where a nearly perfect SFT appears some distance from a GB. In this case, the SFT and GB are not directly connected, yet the SFT still decreases in size (bottom panel of Fig. 4(c)) and eventually disappears. Detailed processes of immobile SFT annihilation are provided in Fig. S3 of *SI*. This SFT elimination signifies interstitial absorption, which could arise from the surrounding bulk region and GB emission. Even though nearly 18% of the SFTs in our simulations are perfect, their structures can be disrupted by adjacent collision cascades or by incoming defects, and conceivably some of them could turn into defective ones with high mobilities. This possible perfect-defective transformation facilitates SFTs reaching GBs, and ultimately annihilation via GB-SFT interaction.

3.3. GB size-dependent defect density

It has been reported in experiments that NC materials with smaller grain sizes have higher tolerance to radiation in comparison with large grained materials [55], which motivates study of the correlation between grain size and defect density. We extract all defects produced by radiation damage and their size distributions in the irradiated systems with grain spacings of $\lambda = 5.7$ nm, 17.1 nm, and 28.4 nm as shown in Fig. 5(a). It can be seen that the system with the smallest λ of 5.7 nm has no defect cluster larger than 500 atoms, whereas in the large λ systems many large clusters appear. The correlation between defect cluster density and λ is shown in Fig. 5(b). The density shows small variation with decreasing λ down to 11.4 nm, below which there is a clear reduction in density at the smallest λ of 5.7 nm. A similar value of 8 nm was reported in recent experiments of nanotwinned Ag by Yu et al. [20], at which the defect density is significantly reduced. Although close agreement is obtained between our simulations and the experiments, it is worth noting that defect annihilation in NC materials is a complex process, dependent on the material, radiation-induced defect type, GB structure, and dose rate [56–58], all of which can influence the defect-sink performance of a GB.

In Fig. 6(a and b), we show the distributions of defect clusters in Σ5(210) systems irradiated to 0.27 dpa with grain spacings of 22.9 nm and 11.4 nm, respectively. One can see that a number of large clusters are formed in the bulk region away from the GB (see Fig. S4 of *SI* for the other GB type and grain spacing). The drastic defect reduction at a small grain spacing of 5.7 nm in Fig. 5(b) suggests a synergistic effect on damage reduction, which is more effective than the sum of two individual GBs. The synergistic effect

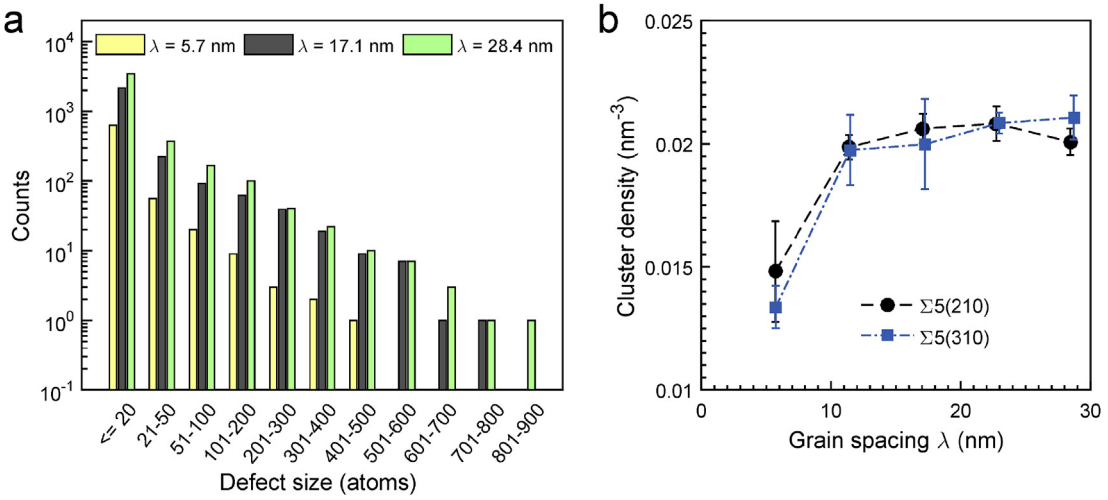

Fig. 5. (a) Statistical distributions of defect size for different Σ5(210) spacing λ. Three independent simulations are performed for each grain spacing λ, and all defects produced at doses from 0.06 dpa to 0.27 dpa are extracted. (b) The density of defect clusters (with size > 1) as a function of λ for both Σ5(210) and Σ5(310) GBs.

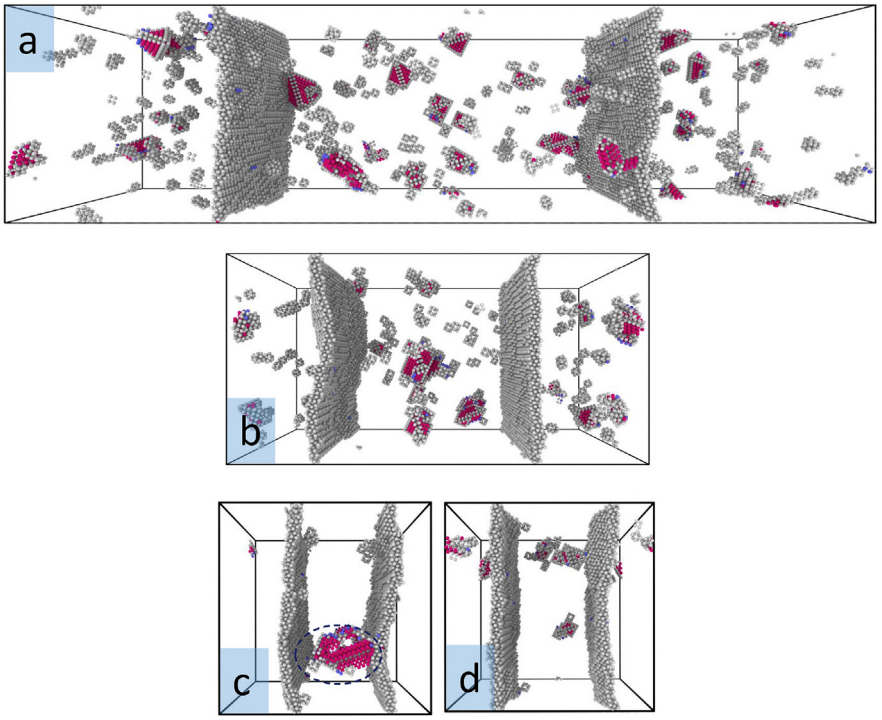

Fig. 6. (a) and (b) spatial distributions of defect clusters in irradiated Σ5(210) systems at 0.27 dpa with λ values of 22.9 nm and 11.4 nm, respectively. (c) Two GBs simultaneously interact with a large SFT at a small λ of 5.7 nm. Small defects are the primary forms of damage (d). Atom color coding is the same as in Fig. 2. (For interpretation of the references to color in this figure legend, the reader is referred to the Web version of this article.)

can be interpreted by Fig. 6(c) which depicts two GBs operating synchronously and cooperatively to interact with a large SFT. This accounts for the irradiated system maintaining only few small-size defects (see Fig. 6(d)). The results suggest an approach to improving material radiation tolerance by optimizing grain size from the standpoint of this synergistic effect.

4. Discussion

In this work, we present the detailed, atomistic evolution of radiation-induced defects in NC-Cu with increasing dose up to 0.27 dpa. The defect density variation with dose is found to consist of two stages, an initial stage of rapid density rise, followed by a saturation stage at which defect creation and annihilation processes are approximately in balance. GBs preferentially absorb interstitials, as has been seen in previous studies, leaving behind a vacancy-rich bulk region. We found that vacancies and clusters rearrange under irradiation and coalesce into stable SFTs. These defects slow the motion of dislocations during mechanical deformation, and are essentially responsible for radiation-induced hardening in NC-Cu. The interstitial-loaded GBs are mobile, fluctuating and strongly interacting with the surrounding defects, thereby the motion of defective GBs further enhances the annihilation of defect clusters.

Our simulations reveal two characteristic mechanisms involved in SFT annihilation. The interaction between interstitial-rich GBs and defective SFTs is the dominant and efficient process for SFT removal, while interstitial recombination appears to contribute more to annihilate immobile, perfect SFTs. The GBs are dynamically resilient during their interaction with defect clusters. In response to the incoming SFTs, the GBs distort their structure and recover after absorbing SFTs in a self-healing manner. It is worth noting that SFTs can also anneal via interaction with low-angle and irradiated coherent twin boundaries [15]. While the detailed process could depend on specific boundary characteristics, the effects of GBs on defect removal and radiation-resistance appear to be quite general. The SFT annihilation-enhanced radiation resistance can also be applied to other FCC metals such as Ag, Ni, and Au, which feature SFTs as the predominant defect type under irradiation. However, due to a high stacking fault energy, Al does not form SFTs under irradiation [28] and its specific damage reduction mechanisms require future investigation.

The diffusion of SFTs near GBs exhibits non-random walk migration characteristics, showing a drift towards the boundary. This directional diffusion suggests an attractive force exerted on the SFTs by interstitial-rich GBs, essentially the same as the elastic interaction between point defects and material interfaces [54]. The drastic defect density reduction at a small grain spacing of 5.7 nm signifies the synergistic effects of GBs on defect annihilation, leading to the interpretation of improved radiation damage tolerance in NC materials compared with their coarse-grain counterparts. On the other hand, small grains suffer rapid radiation-induced growth, so that the overall radiation effects and structural impact may be governed by the competition between efficient defect annealing and simultaneous grain growth. Manipulating the GBs through segregating dopants [59] provides a potential path to stabilize the boundary structure and slow the rate of grain growth. Radiation-induced grain growth is not captured by the current simulations due to the low GB mobility at this low temperature (300 K) and short MD timescale (order of tens of ns). It should be noted that grain growth has been frequently reported for irradiated nanocrystalline materials, and a thermal spike-induced mechanism was proposed by Kaoumi et al. [60].

Our results provide mechanistic insights regarding radiation damage reduction in NC metals, and have important implications for designing and optimizing radiation-resistant nanostructural materials. The observed sharp change of defect density by varying grain spacing represents design guidance on the grain size of Cu, and other FCC metals with low stacking fault energies, subject to irradiation. This observation likely illustrates a general trend in other materials, though the optimal size will depend on the material type, GB characteristics, and other competing effects such as grain growth. These results also motivate investigating the processes and mechanisms of radiation damage reduction in nanocomposites, such as metal-carbon nanotube composites [61], nanolaminates [62–64], and oxide dispersion strengthened materials [65].

5. Summary

Atomistic simulations of radiation damage in nanocrystalline Cu have been performed to experimentally comparable dose levels to investigate GB-mediated defect reduction. The results reveal the details of defect creation, non-random migration, and SFT annealing mechanisms during irradiation. The SFTs induced by radiation damage exhibit preferential migration towards GBs and predominantly annihilate via interactions with GBs. Irradiated GBs with high concentrations of interstitials persistently interact with SFTs, revealing a self-healing nature of NC metals. Moreover, considering the grain size effect, defect cluster density shows a drastic drop when the grain spacing is smaller than 6 nm. Overall, this work demonstrates the atomistic details of defect evolution and reduction mechanisms in irradiated NC metals.

Acknowledgements

M.M.J and P.H.C. contributed equally to this work. P.H.C implemented the simulation model. M.M.J. and P.H.C. conducted the simulations. All authors analyzed the data and wrote the paper. The authors acknowledge support by the Idaho National Laboratory (INL) Nuclear University Consortium (NUC) under the Laboratory Directed Research and Development Grant No. 10-112583, by the US Department of Energy (DOE) NEUP Grant DE-NE0008450, and by the National Science Foundation CAREER Grant DMR-1654548.

Appendix A. Supplementary data

Supplementary data related to this article can be found at https://doi.org/10.1016/j.actamat.2018.05.071.

References

[1] T.D. Shen, S. Feng, M. Tang, J.A. Valdez, Y. Wang, K.E. Sickafus, Enhanced radiation tolerance in nanocrystalline $MgGa_2O_4$, Appl. Phys. Lett. 90 (26) (2007), 263115.
[2] M. Demkowicz, R. Hoagland, J. Hirth, Interface structure and radiation damage resistance in Cu-Nb multilayer nanocomposites, Phys. Rev. Lett. 100 (13) (2008), 136102.
[3] E.M. Bringa, J. Monk, A. Caro, A. Misra, L. Zepeda-Ruiz, M. Duchaineau, F. Abraham, M. Nastasi, S. Picraux, Y. Wang, et al., Are nanoporous materials radiation resistant? Nano Lett. 12 (7) (2011) 3351–3355.
[4] G. Odette, M. Alinger, B. Wirth, Recent developments in irradiation-resistant steels, Annu. Rev. Mater. Res. 38 (2008) 471–503.
[5] I. Beyerlein, A. Caro, M. Demkowicz, N. Mara, A. Misra, B. Uberuaga, Radiation damage tolerant nanomaterials, Mater. Today 16 (11) (2013) 443–449.
[6] G. Watkins, K. Brower, EPR observation of the isolated interstitial carbon atom in silicon, Phys. Rev. Lett. 36 (22) (1976) 1329.
[7] K. Arakawa, K. Ono, M. Isshiki, K. Mimura, M. Uchikoshi, H. Mori, Observation of the one-dimensional diffusion of nanometer-sized dislocation loops, Science 318 (5852) (2007) 956–959.
[8] C. Dai, P. Saidi, Z. Yao, M.R. Daymond, Atomistic simulations of Ni segregation to irradiation induced dislocation loops in Zr-Ni alloys, Acta Mater. 140 (2017) 56–66.
[9] W. Xu, Y. Zhang, G. Cheng, W. Jian, P.C. Millett, C.C. Koch, S.N. Mathaudhu, Y. Zhu, In-situ atomic-scale observation of irradiation-induced void formation, Nat. Commun. 4 (2013) 2288.
[10] K. Yu, Y. Liu, C. Sun, H. Wang, L. Shao, E. Fu, X. Zhang, Radiation damage in helium ion irradiated nanocrystalline Fe, J. Nucl. Mater. 425 (1) (2012) 140–146.
[11] D. Kiener, P. Hosemann, S. Maloy, A. Minor, In situ nano-compression testing of irradiated copper, Nat. Mater. 10 (8) (2011) 608.
[12] R. Barnes, Embrittlement of stainless steels and nickel-based alloys at high temperature induced by neutron radiation, Nature 206 (4991) (1965) 1307–1310.
[13] F. Garner, M. Toloczko, B. Sencer, Comparison of swelling and irradiation creep behavior of fcc-austenitic and bcc-ferritic/martensitic alloys at high neutron exposure, J. Nucl. Mater. 276 (1) (2000) 123–142.
[14] N. Li, K. Hattar, A. Misra, In situ probing of the evolution of irradiation-induced defects in copper, J. Nucl. Mater. 439 (1) (2013) 185–191.
[15] K. Yu, D. Bufford, F. Khatkhatay, H. Wang, M. Kirk, X. Zhang, In situ studies of irradiation-induced twin boundary migration in nanotwinned Ag, Scripta Mater. 69 (5) (2013) 385–388.
[16] J. Li, K. Yu, Y. Chen, M. Song, H. Wang, M. Kirk, M. Li, X. Zhang, In situ study of defect migration kinetics and self-healing of twin boundaries in heavy ion irradiated nanotwinned metals, Nano Lett. 15 (5) (2015) 2922–2927.
[17] Y. Chen, J. Li, K. Yu, H. Wang, M. Kirk, M. Li, X. Zhang, In situ studies on radiation tolerance of nanotwinned cu, Acta Mater. 111 (2016) 148–156.
[18] N. Li, J. Wang, Y. Wang, Y. Serruys, M. Nastasi, A. Misra, Incoherent twin boundary migration induced by ion irradiation in Cu, J. Appl. Phys. 113 (2) (2013), 023508.
[19] Y. Chimi, A. Iwase, N. Ishikawa, M. Kobiyama, T. Inami, S. Okuda, Accumulation and recovery of defects in ion-irradiated nanocrystalline gold, J. Nucl. Mater. 297 (3) (2001) 355–357.
[20] K. Yu, D. Bufford, C. Sun, Y. Liu, H. Wang, M. Kirk, M. Li, X. Zhang, Removal of stacking-fault tetrahedra by twin boundaries in nanotwinned metals, Nat. Commun. 4 (2013) 1377.
[21] M. Samaras, P. Derlet, H. Van Swygenhoven, M. Victoria, Computer simulation

of displacement cascades in nanocrystalline ni, Phys. Rev. Lett. 88 (12) (2002), 125505.
[22] M. Samaras, P. Derlet, H. Van Swygenhoven, M. Victoria, Atomic scale modelling of the primary damage state of irradiated fcc and bcc nanocrystalline metals, J. Nucl. Mater. 351 (1) (2006) 47–55.
[23] X.-M. Bai, A.F. Voter, R.G. Hoagland, M. Nastasi, B.P. Uberuaga, Efficient annealing of radiation damage near grain boundaries via interstitial emission, Science 327 (5973) (2010) 1631–1634.
[24] X.-M. Bai, L.J. Vernon, R.G. Hoagland, A.F. Voter, M. Nastasi, B.P. Uberuaga, Role of atomic structure on grain boundary-defect interactions in Cu, Phys. Rev. B 85 (21) (2012), 214103.
[25] M.J. Demkowicz, O. Anderoglu, X. Zhang, A. Misra, The influence of 3 twin boundaries on the formation of radiation-induced defect clusters in nanotwinned Cu, J. Mater. Res. 26 (14) (2011) 1666–1675.
[26] X.-M. Bai, B.P. Uberuaga, The influence of grain boundaries on radiation-induced point defect production in materials: a review of atomistic studies, JOM 65 (3) (2013) 360–373.
[27] D. Chen, J. Wang, T. Chen, L. Shao, Defect annihilation at grain boundaries in alpha-fe, Sci. Rep. 3 (2013) 1450.
[28] R. Schäublin, Z. Yao, N. Baluc, M. Victoria, Irradiation-induced stacking fault tetrahedra in fcc metals, Phil. Mag. 85 (4–7) (2005) 769–777.
[29] M. Niewczas, R. Hoagland, Molecular dynamic studies of the interaction of a/6 <112> Shockley dislocations with stacking fault tetrahedra in copper. Part II: intersection of stacking fault tetrahedra by moving twin boundaries, Phil. Mag. 89 (8) (2009) 727–746.
[30] E. Martínez, B.P. Uberuaga, I.J. Beyerlein, Interaction of small mobile stacking fault tetrahedra with free surfaces, dislocations, and interfaces in Cu and Cu-Nb, Phys. Rev. B 93 (5) (2016), 054105.
[31] L. Zhang, C. Lu, K. Tieu, Y. Shibuta, Dynamic interaction between grain boundary and stacking fault tetrahedron, Scripta Mater. 144 (2018) 78–83.
[32] K. Nordlund, M. Ghaly, R. Averback, M. Caturla, T.D. de La Rubia, J. Tarus, Defect production in collision cascades in elemental semiconductors and fcc metals, Phys. Rev. B 57 (13) (1998) 7556.
[33] Y. Mishin, M. Mehl, D. Papaconstantopoulos, A. Voter, J. Kress, Structural stability and lattice defects in copper: Ab initio, tight-binding, and embedded-atom calculations, Phys. Rev. B 63 (22) (2001), 224106.
[34] J. Rittner, D. Seidman, <110> symmetric tilt grain-boundary structures in fcc metals with low stacking-fault energies, Phys. Rev. B 54 (10) (1996) 6999.
[35] T. Frolov, D.L. Olmsted, M. Asta, Y. Mishin, Structural phase transformations in metallic grain boundaries, Nat. Commun. 4 (2013) 1899.
[36] L. Zhang, C. Lu, K. Tieu, Atomistic simulation of tensile deformation behavior of σ5 tilt grain boundaries in copper bicrystal, Sci. Rep. 4 (2014) 5919.
[37] F. Aurenhammer, Voronoi diagramsa survey of a fundamental geometric data structure, ACM Comput. Surv. 23 (3) (1991) 345–405.
[38] M. Jin, P. Cao, M.P. Short, Thermodynamic mixing energy and heterogeneous diffusion uncover the mechanisms of radiation damage reduction in single-phase Ni-Fe alloys, Acta Mater. 147 (2018) 16–23.
[39] S. Plimpton, Fast parallel algorithms for short-range molecular dynamics, J. Comput. Phys. 117 (1) (1995) 1–19.
[40] J.F. Ziegler, J.P. Biersack, U. Littmark, The Stopping and Range of Ions in Solids, Pergamon Press, 1985.
[41] S. Nosé, A molecular dynamics method for simulations in the canonical ensemble, Mol. Phys. 52 (2) (1984) 255–268.
[42] W.G. Hoover, Canonical dynamics: equilibrium phase-space distributions, Phys. Rev. 31 (1985) 1695–1697.
[43] M. Norgett, M. Robinson, I. Torrens, A proposed method of calculating displacement dose rates, Nucl. Eng. Des. 33 (1) (1975) 50–54.
[44] M.W. Ullah, Y. Zhang, N. Sellami, A. Debelle, H. Bei, W.J. Weber, Evolution of irradiation-induced strain in an equiatomic NiFe alloy, Scripta Mater. 140 (2017) 35–39.
[45] A. Stukowski, Visualization and analysis of atomistic simulation data with OVITO–the Open Visualization Tool, Model. Simulat. Mater. Sci. Eng. 18 (1) (2009), 015012.
[46] L.A. Zepeda-Ruiz, A. Stukowski, T. Oppelstrup, V.V. Bulatov, Probing the limits of metal plasticity with molecular dynamics simulations, Nature 550 (7677) (2017) 492.
[47] A. Stukowski, Structure identification methods for atomistic simulations of crystalline materials, Model. Simulat. Mater. Sci. Eng. 20 (4) (2012), 045021.
[48] GitHub Data Repository for Nanocrystalline Cu Radiation Manuscript, 2018, https://doi.org/10.5281/zenodo.1239133.
[49] D.L. Olmsted, S.M. Foiles, E.A. Holm, Survey of computed grain boundary properties in face-centered cubic metals: I. grain boundary energy, Acta Mater. 57 (13) (2009) 3694–3703.
[50] B. Uberuaga, R. Hoagland, A. Voter, S. Valone, Direct transformation of vacancy voids to stacking fault tetrahedra, Phys. Rev. Lett. 99 (13) (2007), 135501.
[51] J. Hirth, J. Lothe, Theory of Dislocations, second ed., John Wiley & Sons, 1982.
[52] M. Sabochick, S. Yip, Migration energy calculations for small vacancy clusters in copper, J. Phys. F Met. Phys. 18 (8) (1988) 1689.
[53] E. Martínez, B.P. Uberuaga, Mobility and coalescence of stacking fault tetrahedra in Cu, Sci. Rep. 5 (2015) 9084.
[54] A. Vattré, T. Jourdan, H. Ding, M.-C. Marinica, M. Demkowicz, Non-random walk diffusion enhances the sink strength of semicoherent interfaces, Nat. Commun. 7 (2016) 10424.
[55] M. Rose, A. Balogh, H. Hahn, Instability of irradiation induced defects in nanostructured materials, Nucl. Instrum. Meth. Phys. Res. B 127 (1997) 119–122.
[56] M.A. Tschopp, K. Solanki, F. Gao, X. Sun, M.A. Khaleel, M. Horstemeyer, Probing grain boundary sink strength at the nanoscale: energetics and length scales of vacancy and interstitial absorption by grain boundaries in α-Fe, Phys. Rev. B 85 (6) (2012), 064108.
[57] W. Han, M. Demkowicz, E. Fu, Y. Wang, A. Misra, Effect of grain boundary character on sink efficiency, Acta Mater. 60 (18) (2012) 6341–6351.
[58] B.P. Uberuaga, L.J. Vernon, E. Martinez, A.F. Voter, The relationship between grain boundary structure, defect mobility, and grain boundary sink efficiency, Sci. Rep. 5 (2015) 9095.
[59] A. Khalajhedayati, Z. Pan, T.J. Rupert, Manipulating the interfacial structure of nanomaterials to achieve a unique combination of strength and ductility, Nat. Commun. 7 (2016) 10802.
[60] D. Kaoumi, A. Motta, R. Birtcher, A thermal spike model of grain growth under irradiation, J. Appl. Phys. 104 (7) (2008), 073525.
[61] K.P. So, D. Chen, A. Kushima, M. Li, S. Kim, Y. Yang, Z. Wang, J.G. Park, Y.H. Lee, R.I. Gonzalez, M. Kiwi, E.M. Bringa, L. Shao, J. Li, Dispersion of carbon nanotubes in aluminum improves radiation resistance, Nanomater. Energy 22 (Supplement C) (2016) 319–327.
[62] W. Han, M.J. Demkowicz, N.A. Mara, E. Fu, S. Sinha, A.D. Rollett, Y. Wang, J.S. Carpenter, I.J. Beyerlein, A. Misra, Design of radiation tolerant materials via interface engineering, Adv. Mater. 25 (48) (2013) 6975–6979.
[63] Yinmin Wang, et al., Ductile crystalline–amorphous nanolaminates, Proc. Natl. Acad. Sci. 104 (27) (2007) 11155–11160.
[64] Joseph E. Ludy, Timothy J. Rupert, Amorphous intergranular films act as ultra-efficient point defect sinks during collision cascades, Scripta Mater. 110 (2016) 37–40.
[65] R. Klueh, J. Shingledecker, R. Swindeman, D. Hoelzer, Oxide dispersion-strengthened steels: a comparison of some commercial and experimental alloys, J. Nucl. Mater. 341 (2) (2005) 103–114.